Development of softwood kraft lignin-based conductive carbon for sustainable supercapacitor

Nutthira Pakkang,[1] *Masanori Hori*,[2] *Shiori Suzuki*,[1] *Yasumitsu Uraki*[1]*

[1] Research Faculty of Agriculture, Hokkaido University, Kita 9, Nishi 9, Kita-ku, Sapporo, Hokkaido 060-8589, Japan

[2] Innovative Research Excellence, Honda R&D Co., Ltd., 4630 Shimotakanezawa, Haga-machi, Haga-gun, Tochigi, 321-3393, Japan

* Corresponding author E-mail address: uraki@agr.hokudai.ac.jp

Abstract: Electric double-layer capacitors (EDLCs) are promising devices for sustainable energy storage. However, EDLC components, such as separators and electrodes composed of activated carbon and conductive additives, are derived from fossil resources. To reduce this dependency, an EDLC was assembled using a separator and electrodes derived from hardwood kraft lignin, while still relying on fossil-based carbon black (CB) as the conductive additive. To achieve more sustainable EDLCs, this study developed all the conductive carbon, separator, and electrodes from softwood kraft lignin (SKL). When SKL was carbonized at 900 °C, it showed poor electrical conductivity and was unsuitable as a conductive additive. The carbon structures became more ordered with higher temperatures, and SKL-carbons prepared at 1300–2000 °C showed comparable conductivity to CB. The EDLCs with 1 wt.% of these SKL-carbons exhibited higher capacitance and energy density than reference EDLCs with 1 and 5 wt.% CB. Furthermore, a turbostratic (T) structure formed at 2500 °C, enhancing conductivity and EDLC performance. SKL-carbon prepared at 2800 °C exhibited a graphite structure in addition to the T structure, achieving the highest conductivity (0.54 S cm^{-1}), but the resulting EDLC showed low power density. Thus, SKL-carbon prepared at 2500 °C was the best conductive additive for EDLCs.

Keywords: kraft lignin; thermal graphitization; conductive carbon; electrical double layer capacitors; supercapacitor

1. Introduction

Renewable energy has attracted significant attention as a primary alternative to fossil fuels. However, its availability is often intermittent, depending on environmental conditions (Meng et al. 2024). In this context, energy storage devices are essential to ensure a continuous energy supply from renewable sources. Electric double layer capacitors (EDLCs) have emerged as one of the next-generation energy storage devices owing to their rapid charging capability, high power density, and long lifespan (Liang et al. 2024). The key components of EDLCs include liquid electrolytes, separators, electrodes, and additives that enhance the electrical conductivity of the electrodes. As these components are typically derived from petroleum (Loganathan et al. 2022), replacing them with renewable resources would lead to more sustainable EDLC applications.

Lignin, the most abundant aromatic polymer in nature, holds significant promise in this regard. Among technical lignins, kraft lignins (KLs), specifically softwood KL (SKL) and hardwood KL (HKL), are produced in large quantities—exceeding 27 million metric tons per year (Argyropoulos et al. 2023)—as byproducts of the kraft pulping process (Nadányi et al. 2024). SKL and HKL are distinct polymers due to differences in their monomer constituents and the frequency of interunit linkages, particularly condensed linkages (Fodil et al. 2020; Schlee et al. 2020; Suota et al. 2021). Due to their high carbon content, KLs are promising renewable resources for carbon electrode materials such as carbon fiber (CF) and activated carbon fiber (ACF) with high surface areas (Salmén et al. 2015; Schlee et al. 2019; Schlee et al. 2020). However, other EDLC components, such as separators and conductive additives, have gained relatively little attention (Köhnke et al. 2019). Recently, HKL-based separators were developed through electrospinning and thermostabilization, which was subsequently converted into HKL-based electrodes via carbonization and activation (Pakkang et al. 2020, 2023). The EDLC assembled with these components demonstrated high performance, although commercial carbon black (CB) derived from petroleum and coal (Dai et al. 2022; Jiang et al. 2024) was still used as a conductive additive for the electrodes.

This study aims to develop conductive carbon, in addition to a separator and electrodes, from SKL and to assemble an EDLC using these SKL-based key components. Graphite is a well-known conductive material. Two primary methods have been proposed to convert KL into graphite. One is catalytic graphitization using transition metal catalysts (Lower et al. 2023; Sagues et al. 2019; Yan et al. 2021; Yan et al. 2024), which has the advantage of occurring at relatively low temperatures but faces the demerit of removing residual metallic impurities (Lower et al. 2023). The other involves high-temperature carbonization, which is well-suited

for large-scale production despite its high energy consumption (Meščeriakovė et al. 2022; Rodríguez-Mirasol et al. 1996). When HKL was carbonized at temperatures up to 2800 °C, a mixture of graphite (G) and turbostratic (T) structures was formed (Rodríguez-Mirasol et al. 1996). The G structure displayed well-aligned stacked hexagonal planes, whereas the T structure exhibited randomly aligned planes (Venkatachalam et al. 2020). A similar mixture of G and T structures was also formed from SKL, but its formation required a labor-intensive three-step process: hydrothermal carbonization, molten salt-assisted carbonization, and post-carbonization up to 2400 °C (Meščeriakovė et al. 2022). Notably, the electrical conductivity of the carbons derived from both HKL and SKL was not reported. Furthermore, there have been no studies on the carbonization of SKL at elevated temperatures or its application in EDLCs.

In this study, SKL with low ash content underwent simple high-temperature carbonization up to 2800 °C. The structures of the resulting SKL-carbons were analyzed using X-ray diffraction (XRD) and Raman spectroscopy, and their electrical conductivities were measured and compared with that of commercial CB. Additionally, a separator and an electrode material (i.e., ACF) were prepared from SKL, according to those produced from HKL (Pakkang et al. 2023). EDLC electrodes were fabricated using SKL-carbons as conductive additives and SKL-based ACF and then assembled with the SKL-based separator into EDLCs. The electrochemical performance of the resulting EDLCs was evaluated in comparison with that of reference EDLCs using CB instead of SKL-carbons.

2. Materials and methods

2.1. Materials. SKL was isolated from a black liquor of softwood kraft pulping (Nippon Paper Industries Co., Ltd., Tokyo, Japan) through acid precipitation using hydrochloric acid (HCl) (Huang et al. 2024). The precipitate was collected via vacuum filtration and washed multiple times with distilled water until reaching neutral pH. The obtained SKL was further washed with 0.1 M HCl, followed by filtration and additional washing with distilled water until neutral pH was achieved. The washed SKL was then freeze-dried for three days, resulting in a purified SKL powder.

Polyethylene glycol 500kDa (PEG), hexamethylene tetramine (HEX), acetic acid (AcOH), dimethylformamide (DMF), and carboxymethyl cellulose (CMC) were purchased from FUJIFILM Wako Pure Chemical Industries, Co., Ltd., Osaka, Japan. An ionic liquid electrolyte, 1-ethyl-3-methylimidazolium tetrafluoroborate ($EmimBF_4$, >99.0%), was purchased from Proionic GmbH. Grambach, Austria. CB was obtained from Alfa Aesar, Thermo Fisher Scientific Inc., Heysham, UK.

2.2. Preparation of SKL-Carbons as Conductive Materials. SKL was first desalted with dilute acid using a practical and cost-effective purification method (Da Silva et al. 2023; Sharma et al. 2024) to yield a purified SKL powder with a low ash content (0.25 wt.%). This step is necessary because inorganic impurities, such as sodium, calcium, and sulfur, (Enengl et al. 2021) can interfere with the structural ordering during the carbonization process. In addition, the purified SKL powder requires thermostabilization to increase its glass transition temperature (Bhattacharyya et al. 2020), ensuring that it remains in its powder form during high-temperature carbonization. Thus, air oxidation was employed as a simple method to impart thermosetting character to lignin (Köhnke et al. 2019), as follows.

A total of 60 g of the purified SKL powder was placed in a crucible and heated in air at a heating rate of 0.5 °C min^{-1} with a holding time of 1 h at 250 °C, followed by natural cooling to room temperature (RT, 25 °C), resulting in a thermostabilized SKL powder. The mass after thermostabilization was approximately 40 g, corresponding to the yield of 70 wt.%.

The thermostabilized SKL powder was equally divided and carbonized at five different temperatures: 900, 1300, 2000, 2500, and 2800 °C. The carbonization at 900 °C was performed in a muffle furnace (KDF-S90, DENKEN-HIGHDENTAL Co., Ltd., Kyoto, Japan) at a heating rate of 3 °C min^{-1} under a N_2 flow of 0.5 L min^{-1}. At temperatures between 1300 and 2800 °C, carbonization was performed in another muffle furnace (SCC-U-80/150, KURATA GIKEN Co., Ltd., Tachikawa, Japan). The furnace was first evacuated to 60 Pa and then filled with Ar gas at atmospheric pressure. Upon reaching the target temperature at a heating rate of 5 °C min^{-1}, the temperature was held for 1 h. After natural cooling to RT, the pressure inside the furnace was controlled via an adjusted Ar flow to maintain a constant atmospheric pressure throughout the process. The obtained carbon materials were ground into a fine powder using a mortar and pestle and sieved through a 90 μm mesh. This carbon, referred to as SKL-carbon, is denoted as SKL-"carbonization temperature." For example, SKL-900 refers to SKL-carbon obtained by carbonizing at 900 °C.

2.3. Carbon Structure Analysis. XRD (SmartLab, Rigaku Co., Ltd., Tokyo, Japan) analysis was conducted for SKL-carbons and CB using a SmartLab diffractometer (Rigaku Co., Ltd., Akishima, Tokyo, Japan) with CuKα radiation (λ = 0.15406 nm) at 45 kV and 200 mA. The XRD patterns were recorded over a 2θ range of 10–60° at a scan rate of 4° min^{-1}. The average crystallite size (L_c) was determined using the following Equation (1) (Badenhorst et al. 2020; Li et al. 2021):

$$L_c = K\lambda / \beta\cos\theta \quad (1)$$

where K = 0.94, θ is the diffraction angle, and β is the peak width at half-maximum intensity.

Raman spectroscopy was also employed to characterize the structure of SKL-carbons and CB using an inVia Reflex spectrometer (RENISHAW plc., Gloucestershire, UK) with a 532 nm excitation laser. The laser power was set to 0.5 mW, and the scan time was 15 s. The lateral crystallite size (L_a) was calculated using Equation (2) (Zhou et al. 2023):

$$L_a = 2.4\times10^{-10}\ \lambda^4\ (A_D/A_G)^{-1} \quad (2)$$

where λ is the wavelength (nm) of the laser used, and A_D/A_G is the integrated area ratio of the D-band and G-band in the Raman spectra.

2.4. Electrical Conductivity Measurement. The electrical conductivity of SKL-carbons was determined from the measured bulk electrical resistance (Autolab PGSTAT302N FRA32M, Metrohm Autolab B.V., Tokyo, Japan). A 100 mg of the SKL-carbon was placed between two Al sheets and loaded into an EDLC measurement cell (2E-CELL-SUS, Eager Corp., Osaka, Japan). The measurements were performed under an applied voltage of 10 mV over a frequency range from 600 kHz to 400 Hz. Each sample was tested three times. The electrical conductivity (σ, S cm^{-1}) was calculated using the following Equation (3):

$$\sigma = h\ /\ AR \quad (3)$$

where h is the height of the packed sample (cm), A is the base area of the measurement cell (cm^2), and R is the electrical resistance (Ω).

2.5. Surface and Pore Characterization and Density Measurement. The surface area of SKL-carbons was characterized using a surface area analyzer (Autosorb-1, Quantachrome Instruments Japan Co., Ltd., Tokyo, Japan). The specific surface area was calculated using the Brunauer–Emmett–Teller (BET) model, based on the adsorption isotherm in the relative pressure ($P\ P_0^{-1}$) range of 0.02–0.30 (Pakkang et al. 2023). Additionally, the internal and external surface areas were estimated using the *t*-plot method in the $P\ P_0^{-1}$ range of 0.20–0.50. The average pore size and its distribution were determined from the adsorption isotherms using the quenched solid density functional theory (Fu et al. 2021). The densities of SKL-carbons and CB were evaluated using a tapped density measurement (Napiórkowska et al. 2019).

2.6. Preparation of SKL-Separator. An EDLC separator was prepared from SKL according to the previous method (Pakkang et al. 2023). Briefly, the purified SKL powder was mixed with PEG and HEX in a DMF/AcOH binary solvent. The mixture was stirred at 80 °C for 2 h and electrospun from a 5 mL syringe equipped with a metal needle (diameter: 1.3 mm, 18 gauge). The electrospinning conditions were as follows; applied voltage: 18 kV, needle tip–collector distance: 13 cm, and a solution flow rate: 2 mL h^{-1}. The obtained SKL fiber mat was thermostabilized at 250 °C at a heating rate of 2 °C min^{-1}. The yield of the thermostabilized SKL fiber mat was 75 wt.%. The mat with a thickness of 60 μm was cut into a circular shape with a diameter of 18 mm and used directly as the SKL separator.

2.7. Preparation of SKL-Electrode. ELDC electrodes were also prepared from SKL according to the previous method (Pakkang et al. 2023). The thermostabilized SKL fiber mat (cf. *Section 2.6*) was carbonized in a furnace at 900 °C at a heating rate of 3 °C min^{-1} under a N_2 flow of 0.5 L min^{-1}, and the temperature was maintained for 1 h. Steam (total 10 g of water) was then introduced into the furnace along with N_2 gas, and the resulting carbon material underwent steam activation at 900 °C for 1 h. The yield of the resulting ACF mat was 10 wt.% based on the thermostabilized mat.

The typical particle size for commercially available activated carbon products is 90 μm or less, which is essential for fabricating an electrode with low surface roughness and achieving good contact at the interface between the electrode and the separator (Pakkang et al. 2023). Hence, the ACF mat was ground into a fine powder using a mortar and pestle and sieved through a 90 μm mesh in the similar manner to SKL-carbons (cf. *Section 2.2*). The average particle diameter of 150 particles was determined using an optical microscope (Violet Laser Color 3D Profilometer VK-9500, Keyence, Osaka, Japan). Three points at the edge of each particle were selected to make a regular triangle, and the diameter for the circumscribed circle of the triangle was considered as the particle diameter. The ACF fine powder was then mixed with 1 or 5 wt.% of conductive carbon (either the fine powder of SKL-carbons or CB) through grinding using a mortar and pestle for 15 min. Subsequently, a 2% CMC aqueous solution was added to the powder mixture to obtain a CMC content of 10 wt.% in the total solution, and the mixture was ground for another 15 min. The resulting slurry was cast on an Al sheet (thickness: 100 μm, Nilaco Co., Ltd., Tokyo, Japan) using a doctor blade (casting thickness: 50 μm, Sangyo Co., Ltd., Tokyo, Japan) and dried overnight in an oven at 105 °C. The coated Al sheet was cut into a circular shape with a diameter of 16 mm and used as the SKL electrode.

2.8. EDLC Assembly. The SKL separator and electrodes were soaked in $EmimBF_4$ as a liquid electrolyte under vacuum for 2 h. The Al side of the electrode was placed at the bottom of the measurement cell (2E-CELL-SUS, Eager Corp., Osaka, Japan), and the SKL separator was layered on it. The cast side of the other electrode was then placed on it. All the EDLCs were assembled in a glove box filled with Ar gas.

2.9. Electrochemical Characterization of EDLCs. An electrochemical workstation (Autolab PGSTAT302N FRA32M, Metrohm Autolab B.V., Tokyo, Japan) was used to assess the electrochemical performance of the EDLCs. Similar to the previous report (Pakkang et al. 2023), the area of the cyclic voltammogram (CV) with a scan rate of 0.05 V s^{-1} and the discharge slope of the galvanostatic charge-discharge (GCD) profiles at current density of 1 A g^{-1} were used to calculate the specific capacitance of EDLCs in the potential window of 0–3.5 V. An alternating current (AC) amplitude of 10 mV was used to measure the impedance between 100 kHz and 1 Hz using electrochemical impedance spectroscopy (EIS). The charge transfer resistance (R_{ct}) and the equivalent series resistance (R_s) were estimated from the diameter of the semicircle and intercept on the Z' axis of the Nyquist plots, respectively. According to previous studies (Pakkang et al. 2020, 2023), an energy density (E, Wh kg^{-1}) was estimated with Equation (4):

$$E = 1/8\ CV^2 \tag{4}$$

where C (F g^{-1}) is the specific capacitance calculated from the GCD measurement, V is the maximum voltage window (3.5 V).

A power density (P, kW kg^{-1}) was also estimated from the GCD measurement with two Equations (5) (Pakkang et al. 2023) and (6) (Lang et al. 2019). The power density in Equation (5) expresses the electrical power delivered from the electrodes at the initial discharging time ($P_{initial}$), whereas that in Equation (6) is related to the average power delivered over the entire discharge period (P_{ave}).

$$P_{initial} = i(V - V_{drop})^2 / 2mV_{drop} \tag{5}$$

where i (A) is a constant current, m (g) is the total weight of the active mass in electrodes, V_{drop} (V) is the voltage drop obtained from the gap between 3.5 V and the beginning of the discharge.

$$P_{ave} = E \times 3600 / \Delta t \tag{6}$$

where Δt (s) is the discharge time and 3600 is used for the unit conversion from watt-hours to watt-seconds.

3. Results and discussion

3.1. Structural Properties of SKL-Carbons. Figure 1a shows the XRD patterns of SKL-carbons. The carbon prepared at 900 °C shows two broad peaks: a larger peak at 23.0° and a smaller peak at approximately 44°. The larger peak gradually shifted to 25.0° upon increasing the carbonization temperature to 2000 °C, suggesting that the carbon structure was more ordered, but not graphitized. Based on the larger peak, the L_c was calculated for SKL-carbons prepared at 900–2000 °C, and it was almost consistent at 7 nm (Figure 1d). In contrast, the larger peak of SKL-2500 was sharpened and further shifted to 26.0°, clearly indicating the formation of a turbostratic (T) structure (Fogg et al. 2020). This peak was divided into a broad peak for the amorphous (A) structure and a sharp peak for the T structure, as shown in Figure 1b. The L_c was calculated from the deconvoluted T peak and was found to be ten times higher than those of SKL-carbons prepared at 900–2000 °C. This significant increase in the L_c should be attributed to the T structure formed at 2500 °C. In the deconvoluted XRD pattern of SKL-2800 (Figure 1b), a new small peak was observed at 26.4°, corresponding to graphite (G) (Kim et al. 2024; Yuan et al. 2022), in addition to the T peak. This indicates that SKL-2800 consists of both T and G structures. L_c, calculated from the deconvoluted T peak, was reduced by nearly half compared to that of SKL-2500 (Figure 1b). This might be because the hexagonal layers in the T structure began to break away and reformed into a more aligned and packed G structure during the carbonization at 2800 °C.

The Raman spectra of all SKL-carbons (Figure 1c) and CB (Figure S1) show a disorder-related D-band at 1350 cm^{-1} and a G-band at 1580 cm^{-1} that is characteristic of native graphite (Yan et al. 2020), while a D'-band at 1620 cm^{-1}, referring to the defects in graphene (Escobar et al. 2024), was not observed. Furthermore, when the carbonization temperature exceeded 2000 °C, a 2D band at 2700 cm^{-1}, indicative of graphene (Melníková-Komínková et al. 2022), appeared. By contrast, in the deconvoluted XRD pattern of SKL-2000 (Figure S2), a small peak was found at 25.7°, however, which is a different peak from the T peak typically detected at 26.0° (Fogg et al. 2020). These results suggest that 2000 °C is the threshold temperature to form graphene from SKL but is not enough to develop the T structure. As the temperature further increased to 2500 and 2800 °C, the 2D band was sharpened and the intensity was increased, suggesting the development of graphene formation. In addition, L_a continuously

increased with increasing carbonization temperature (Figure 1d), as calculated from the area ratio of the D and G bands (A_D/A_G, Figure 1c).

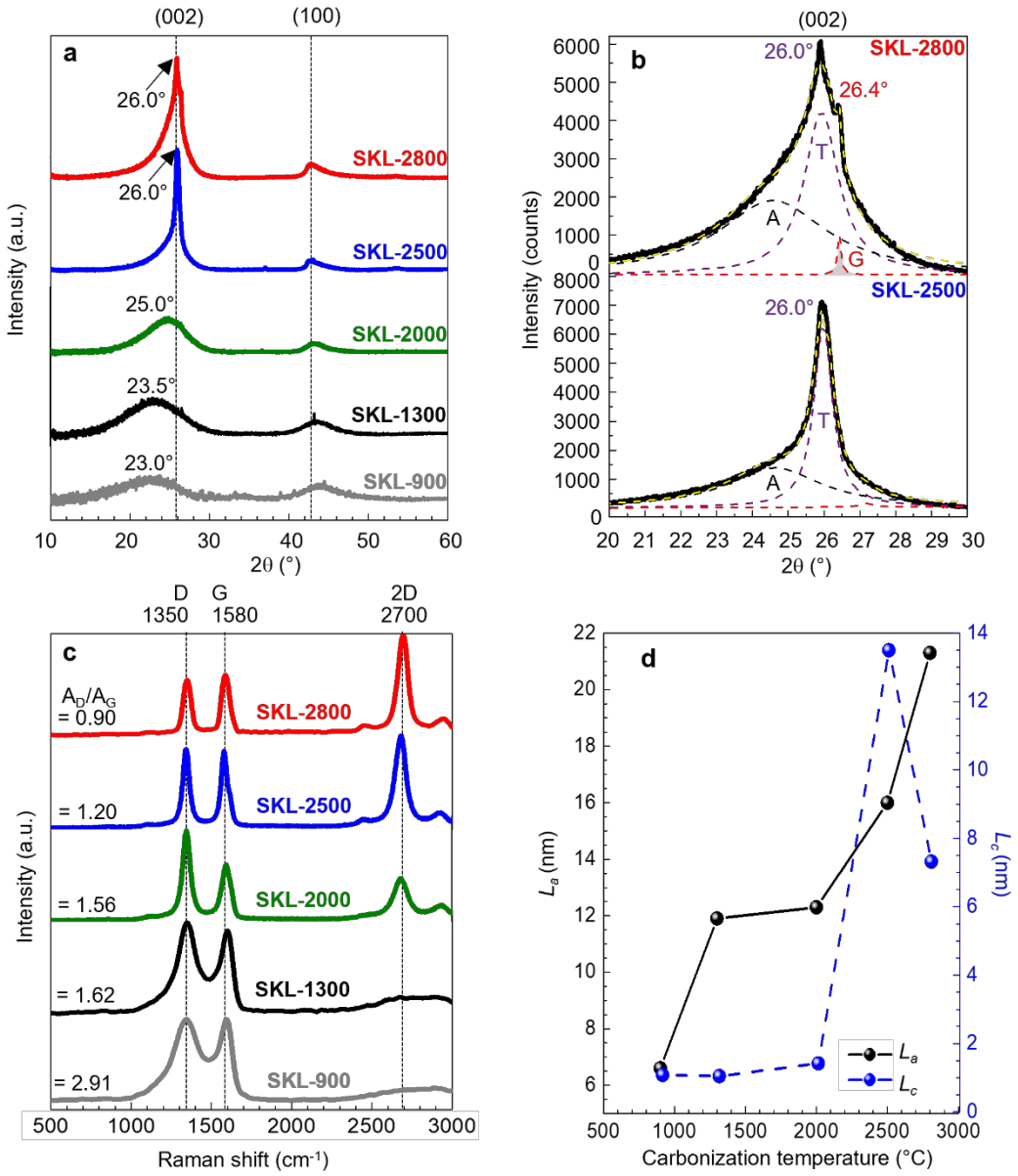

Figure 1: XRD patterns of SKL carbonized at 900–2800 °C (a), their deconvolution of SKL-2500 and SKL-2800 ranging from 20–30° fitted with Voigt function (b), Raman spectra with the integrated area ratio of the D-band and G-band; A_D/A_G (c), and changes in the lateral crystalline size; L_a (black solid line) and the stacking height; L_c (blue dashed line) of SKL-carbons with increasing the carbonization temperatures.

3.2. Electrical Conductivity and Physical Property of SKL-Carbons. The electrical conductivity of CB used in this study was 0.21 S cm^{-1}, which is comparable to those of typical CBs measured (Pantea et al. 2003). Figure 2 shows the change in the conductivity of SKL-

carbons with increasing the carbonization temperatures. Among CB and SKL-carbons, SKL-900 showed the lowest conductivity (0.09 S cm^{-1}) and was considered unsuitable as a conductive additive for EDLC applications. The conductivity increased with increasing carbonization temperature, and SKL-1300, SKL-2000, and SKL-2500 exhibited comparably high CB conductivities. SKL-2800 exhibited remarkably high conductivity of 0.54 S cm^{-1}, probably due to the enhanced graphene formation (Figure 1c) in addition to the G structure development (Figure 1b). These results indicate that SKL-carbons prepared above 1300 °C can be practical conductive carbons to replace petroleum-based commercial CBs.

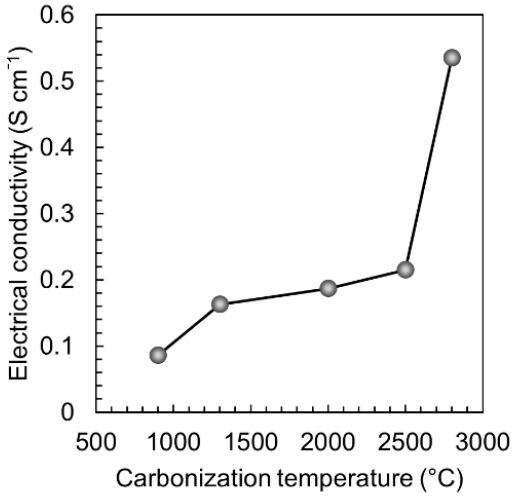

Figure 2: Electrical conductivity of SKL-carbons prepared at various carbonization temperatures from 900 to 2800 °C.

The average particle diameters of SKL-carbons ranged from 0.77 to 0.84 μm (Figure S3), which are considerably larger than that of CB (0.042 μm). As shown in Table 1, SKL-carbons have lower specific surface areas and total pore volumes than commercial CB. Consequently, the density of SKL-carbons was more than five times higher than that of CB. Furthermore, the density gradually increased with increasing carbonization temperature, probably owing to the reduced pore volume (Table S1). A significant advantage of SKL-carbon is that, when used at a constant mass for electrode preparation, its higher density than that of CB allows the resulting electrode to have a lower volume.

Table 1: Tapped density and surface properties of SKL-carbon prepared at various carbonization temperatures and commercial CB.

Carbon samples	Tapped density [a] ($kg\ m^{-3}$)	Specific surface area [b] ($m^2\ g^{-1}$)	Total pore volume ($cm^3\ g^{-1}$)
CB	90	63.4	6.05×10^{-3}
SKL-1300	500	15.6	2.52×10^{-3}
SKL-2000	520	16.5	2.73×10^{-3}
SKL-2500	550	14.7	2.73×10^{-3}
SKL-2800	570	17.9	1.78×10^{-3}

[a] Measured according to the previous method (Napiórkowska et al. 2024). [b] Determined using the BET model.

3.3. Electrochemical Performance of EDLCs with SKL-Carbons as Conductive Additives. The electrodes were prepared from an SKL-based ACF with 1 wt.% of SKL-carbons obtained above 1300 °C as conductive additives and then assembled with an SKL-based separator to fabricate EDLCs. The resistances (R) were estimated by Nyquist plots (Figure 3a), while specific capacitances (C) were determined from CV and GCD curves (Figure 3b,c). Table 2 summarizes the capacitances and resistances besides the energy density (E), average power density (P_{ave}), and initial power density ($P_{initial}$). P_{ave} is the average power delivered during the entire discharge period. By contrast, $P_{initial}$ represents the maximum power output at the start of the discharge, which corresponds to the rapid power-release capability of the EDLCs.

The EDLC performance, especially C and E, improved with higher carbonization temperatures of the SKL carbons used. The EDLC with SKL-2800 exhibited the highest C and E among those with SKL-carbons, but its P_{ave} and $P_{initial}$ were the lowest (Table 2). These low power densities were caused by the high voltage drop (V_{drop}) at the beginning of the discharge as shown in the expanded GCD profile (Figure 3d). As SKL-2800 is composed of a mixture of T- and G-structures (Figure 1b), the resulting structural heterogeneity may impede efficient electrolyte ion transport. This was supported by the high V_{drop} (Figure 3d) and twice the charge transfer resistance (R_{ct}) of the other SKL-carbons (Table 2). In contrast, the EDLC with SKL-2500 exhibited $P_{initial}$ over three times higher than that with SKL-2800, in addition to the second-highest C and E among those with SKL-carbons. This excellent performance can be attributed to the uniform T structure of SKL-2500. Therefore, SKL-2500 was found to be the best conductive additive for EDLCs among all SKL-carbons.

The electrochemical performance (*C* and *E*) of the EDLCs with 1 wt.% SKL-carbons was better than that of reference EDLCs with 1 wt.% and 5 wt.% CB (Table 2). This superior performance may be attributed to the higher density of SKL−carbon compared to that of CB (Table 1). At the same mass loading, CB occupies a larger volume in the electrode and may block pores in the active material (i.e., ACF) than SKL-carbons. As a result, the number of available sites for adsorption and desorption of ions is reduced, which consequently lowers the *C* and *E* of the EDLCs.

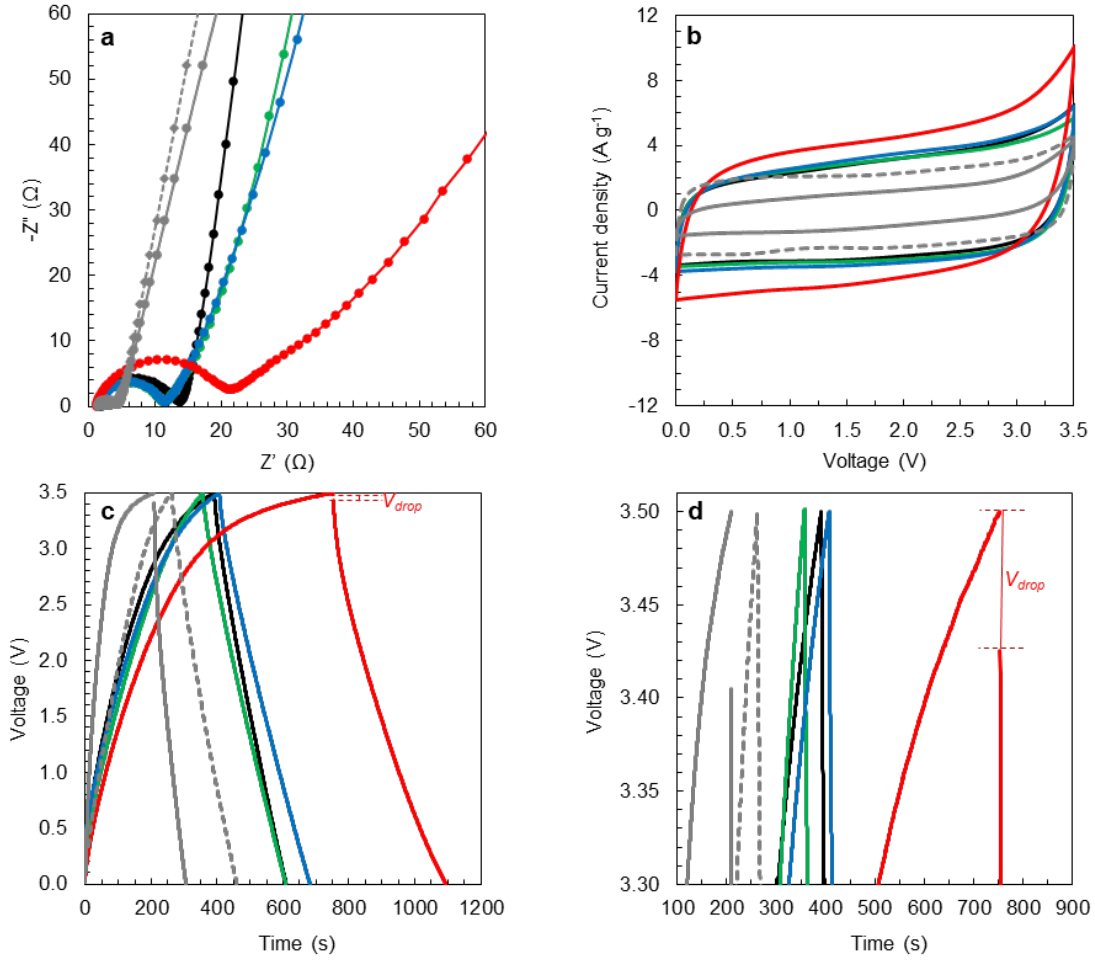

Figure 3: Electrochemical performance of EDLCs with 1 wt.% of SKL-1300 (black), SKL-2000 (green), SKL-2500 (blue), SKL-2800 (red), and CB (gray line) and 5 wt.% of CB (gray dash-line). Nyquist plots (a), CV curves at a scan rate of 0.05 V s^{-1} (b), GCD curves at a current density of 1 A g^{-1} (c), and the expanded GCD curves with a vertical axis range of 3.30–3.50 V for displaying V_{drop} (d).

Table 2: Electrochemical performance of EDLCs using different conductive carbon materials.

Conductive material	Additive (wt.%)	C_{CV} [a] (F g^{-1})	C_{GCD} [b] (F g^{-1})	R_s [c] (Ω)	R_{ct} [d] (Ω)	E [e] (Wh kg^{-1})	$P_{initial}$ [f] (kW kg^{-1})	P_{ave} [g] (W kg^{-1})
SKL-1300	1	119	132	1.1	12.0	56	134	926
SKL-2000	1	123	149	1.2	9.7	63	166	908
SKL-2500	1	133	165	1.4	9.6	70	122	923
SKL-2800	1	173	200	1.2	19.7	85	39	898
CB	1	44	62	1.0	7.7	26	30	983
CB	5	91	114	1.2	1.9	49	178	887

[a] Gravimetric specific capacitance calculated from CV profiles. [b] Specific capacitance calculated from GCD profiles. [c] Equivalent series resistance and [d] charge transfer resistance estimated from the Nyquist plots. [e] Energy density. [f] Power density at initial discharge time and [g] average power density over the entire discharge period.

4. Conclusions

As the carbonization temperature increased from 900 to 2800 °C, the structure of SKL-carbons became more ordered, and the electrical conductivity improved. A turbostratic (T) structure began to form at 2500 °C, while a graphite (G) structure was generated only at 2800 °C. The obtained SKL-2800, with a mixture of T and G structures, exhibited the highest conductivity among all SKL-carbons, but its structural heterogeneity led to less effective power delivery of the assembled EDLC. Conversely, SKL-2500, with its homogeneous T structure, achieved an excellent overall EDLC performance, even when only 1 wt.% was used as a conductive additive, it had a comparable effect to 5 wt.% of commercial CB. These results demonstrate that SKL-2500 is a promising and sustainable alternative to conventional CBs derived from fossil resources. Furthermore, because a small amount of additives is required, SKL-2500 can contribute to the construction of lightweight and high-performance EDLCs, particularly in the fields of vehicle and aerospace applications.

Acknowledgements:

The authors would like to thank Dr. Y. Yamanouchi in The High Brilliance X-ray Laboratory at Hokkaido University for her assistance with XRD measurements and J. Nishiyama in Wood Chemistry Laboratory at Hokkaido University for his assistance with particle size distribution measurements.

Author contribution:

Nutthira Pakkang: writing—original draft, visualization, methodology, investigation, formal analysis, data curation. Masanori Hori: resources, investigation, project administration. Shiori Suzuki: writing—review and editing, supervision, funding acquisition. Yasumitsu Uraki: Conceptualization, writing—review and editing, supervision, funding acquisition.

Research funding:

This work is financially supported by a Grant from Honda R&D Co., Ltd., JSPS KAKENHI (Grant Number: JP23H03828), and JST ALCA-Next (Grant Number: JPMJAN23C3).

Conflict of interest statement:

The authors declare no conflicts of interest regarding this article.

References

Argyropoulos, D.D.S., Crestini, C., Dahlstrand, C., Furusjo, E., Gioia, C., Jedvert, K., Henriksson, G., Hulteberg, C., Lawoko, M., Pierrou, C., Samec, J.S.M., Subbotina, E., Wallmo, H., Wimby, M. (2023). Kraft Lignin: A valuable, sustainable resource, opportunities and challenges. *ChemSusChem* 16: e202300492.

Badenhorst, C., Santos, C., Lázaro-Martínez, J., Białecka, B., Cruceru, M., Guedes, A., Guimarães, R., Moreira, K., Predeanu, G., Suárez-Ruíz, I., Cameán, I., Valentim, B., Wagner, N. (2020). Assessment of graphitized coal ash char concentrates as a potential synthetic graphite source. *Minerals* 10: 986.

Bhattacharyya, S., Matsakas, L., Rova, U., Christakopoulos, P. (2020). Melt stable functionalized organosolv and kraft lignin thermoplastic. *Processes* 8: 1108.

Da Silva, P.M., Pasa, V.M.D. (2023). Upgrading of kraft lignin with phosphoric acid purification: A promising route for the synthesis of renewable epoxy resins. *Ind. Crops Prod.* 204: 117202.

Dai, L., Shan, M., Li, J., Chen, J., Lv, W., Fu, P., Ma, H., Wang, H. (2022). Purification and reuse of carbon black wastewater of acetylene production from natural gas by microchannel filtration. *Process Saf. Environ. Prot.* 162: 219–229.

Enengl, C., Lumetzberger, A., Duchoslav, J., Mardare, C.C., Ploszczanski, L., Rennhofer, H., Unterweger, C., Stifter, D., Fürst, C. (2021). Influence of the carbonization temperature on the properties of carbon fibers based on technical softwood kraft lignin blends. *Carbon Trends* 5: 100094.

Escobar Veras, S., Espada, E., Collazo, S., Grau, M., Katiyar, R., Makarov, V.I., Weiner, B.R., Morell, G. (2024). Hydrogenated graphene systems: A novel growth and hydrogenation process. *Carbon Trends* 15: 100360.

Fodil Cherif, M., Trache, D., Brosse, N., Benaliouche, F., Tarchoun, A.F. (2020). Comparison of the physicochemical properties and thermal stability of organosolv and kraft lignins from hardwood and softwood biomass for their potential valorization. *Waste Biomass Valor.* 11: 6541–6553.

Fogg, J.L., Putman, K.J., Zhang, T., Lei, Y., Terrones, M., Harris, P.J.F., Marks, N.A., Suarez-Martinez, I. (2020). Catalysis-free transformation of non-graphitising carbons into highly crystalline graphite. *Commun. Mater.* 1: 47.

Fu, S., Fang, Q., Li, A., Li, Z., Han, J., Dang, X., Han, W. (2021). Accurate characterization of full pore size distribution of tight sandstones by low-temperature nitrogen gas adsorption and high-pressure mercury intrusion combination method. *Energy Sci. Eng.* 9: 80–100.

Huang, M., Zhu, L., Li, J., Ma, Z. (2024). Recovery of kraft lignin from industrial black liquor for a sustainable production of value-added light aromatics by the tandem catalytic pyrolysis. *J. Clean. Prod.* 446: 141388.

Jiang, H., Shao, J.A., Hu, Q., Zhu, Y., Cheng, W., Zhang, J., Fan, T., Yu, J., Yang, H., Zhang, X., Chen, H. (2024). Carbon black production characteristics and mechanisms from pyrolysis of rubbers. *Fuel Process. Technol.* 253: 108011.

Kim, Y.S., Hanif, M.A., Song, H., Kim, S., Cho, Y., Ryu, S.-K., Kim, H.G. (2024). Wood-derived graphite: A sustainable and cost-effective material for a wide range of industrial applications. *Crystals* 14: 309.

Köhnke, J., Gierlinger, N., Prats-Mateu, B., Unterweger, C., Solt, P., Mahler, A.K., Schwaiger, E., Liebner, F., Gindl-Altmutter, W. (2019). Comparison of four technical lignins as a resource for electrically conductive carbon particles. *BioRes*. 14: 1091–1109.

Lang, J., Zhang, X., Liu, L., Yang, B., Yang, J., Yan, X. (2019). Highly enhanced energy density of supercapacitors at extremely low temperatures. *J. Power Sources* 423: 271–279.

Lee, S.-M., Lee, S.-H., Roh, J.-S. (2021). Analysis of activation process of carbon black based on structural parameters obtained by XRD analysis. *Crystals* 11: 153.

Li, Q., Hu, C., Li, M., Truong, P., Li, J., Lin, H.-S., Naik, M.T., Xiang, S., Jackson, B.E., Kuo, W., Wu, W., Pu, Y., Ragauskas, A.J., Yuan, J.S. (2021). Enhancing the multi-functional properties of renewable lignin carbon fibers via defining the structure–property relationship using different biomass feedstocks. *Green Chem.* 23: 3725–3739.

Liang, L., Li, L., Chen, R., Meng, J., Liu, H., Guo, C., Bao, W., Yao, D., Zhang, G., Yu, F. (2024). Research advances in plant-derived activated carbon for electric double layer capacitors. *J. Alloys Compd.* 992: 174641.

Loganathan, N.N., Perumal, V., Pandian, B.R., Atchudan, R., Edison, T.N.J.I., Ovinis, M. (2022). Recent studies on polymeric materials for supercapacitor development. *J. Energy Storage* 49: 104149.

Lower, L., Dey, S.C., Vook, T., Nimlos, M., Park, S., Sagues, W.J. (2023). Catalytic graphitization of biocarbon for lithium-ion anodes: A minireview. *ChemSusChem* 16: e202300729.

Melníková-Komínková, Z., Valeš, V., Frank, O., Kalbáč, M. (2022). Evolution of the Raman 2D' mode in monolayer graphene during electrochemical doping. *Microchem. J.* 181: 107739.

Meng, X., Zhang, S., Liu, H., Zhou, S. (2024). A method of energy storage capacity planning to achieve the target consumption of renewable energy. *J. Energy Storage* 97: 112993.

Meščeriakovė, S.-M., Sermyagina, E., Mäkilä, E., Meščeriakovas, A., Karhunen, T., Nissinen, V., Suvanto, S., Lähde, A. (2022). Kraft lignin-derived carbon sheets produced by molten salt-assisted thermal treatment – Graphitization behavior of the sheet structures. *Diam. Relat. Mater.* 127: 109146.

Nadányi, R., Zinovyev, G., Majerčiak, M., Štosel, M., Jablonský, M., Ház, A. (2024). Optimizing hardwood lignin precipitation from kraft black liquor: A study of temperature and pH effects. *Forests* 15: 1028.

425 Napiórkowska, A., Aktaş, H., Szpicer, A., Górska-Horczyczak, E., Kurek, M.A. (2024).
426 Optimization of oat protein and gum arabic microcapsules containing juniper essential
427 oil using response surface methodology. *Food Bioprod. Process.* 145: 203–216.

428 Pakkang, N., Kumar, M., Taira, S., Koda, K., Shigetomi, K., Uraki, Y. (2020). Preparation of
429 kraft lignin-based activated carbon fiber electrodes for electric double layer capacitors
430 using an ionic liquid electrolyte. *Holzforschung* 74: 577–588.

431 Pakkang, N., Suzuki, S., Shigetomi, K., Uraki, Y. (2023). Assembly of electric double-layer
432 capacitors with hardwood kraft lignin-based electrodes and separator together with ionic
433 liquid electrolyte. *Holzforschung* 77: 119–126.

434 Pantea, D., Darmstadt, H., Kaliaguine, S., Roy, C. (2003). Electrical conductivity of conductive
435 carbon blacks: Influence of surface chemistry and topology. *Appl. Surf. Sci.* 217: 181–
436 193.

437 Rodríguez-Mirasol, J., Cordero, T., Rodríguez, J.J. (1996). High-temperature carbons from
438 kraft lignin. *Carbon* 34: 43–52.

439 Sagues, W.J., Jain, A., Brown, D., Aggarwal, S., Suarez, A., Kollman, M., Park, S.,
440 Argyropoulos, D.S. (2019). Are lignin-derived carbon fibers graphitic enough? *Green*
441 *Chem.* 21: 4253–4265.

442 Salmén, L., Bergnor, E., Olsson, A.-M., Åkerström, M., Uhlin, A. (2015). Extrusion of
443 Softwood kraft lignins as precursors for carbon fibres. *BioRes.* 10: 7544.

444 Schlee, P., Hosseinaei, O., Baker, D., Landmér, A., Tomani, P., Mostazo-López, M.J., Cazorla-
445 Amorós, D., Herou, S., Titirici, M.-M. (2019). From waste to wealth: from kraft lignin
446 to free-standing supercapacitors. *Carbon* 145: 470–480.

447 Schlee, P., Hosseinaei, O., O'Keefe, C.A., Mostazo-López, M.J., Cazorla-Amorós, D., Herou,
448 S., Tomani, P., Grey, C.P., Titirici, M.-M. (2020). Hardwood versus softwood kraft lignin
449 – Precursor-product relationships in the manufacture of porous carbon nanofibers for
450 supercapacitors. *J. Mater. Chem. A* 8: 23543–23554.

451 Sharma, M., Marques, J., Simões, A., Donato, M.M., Cardoso, O., Gando-Ferreira, L.M. (2024).
452 Optimization of lignin precipitation from black liquor using organic acids and its
453 valorization by preparing lignin nanoparticles. *Int. J. Biol. Macromol.* 269: 131881.

Suota, M.J., da Silva, T.A., Zawadzki, S.F., Sassaki, G.L., Hansel, F.A., Paleologou, M., Ramos, L.P. (2021). Chemical and structural characterization of hardwood and softwood LignoForce™ lignins. *Ind. Crops Prod.* 173: 114138.

Venkatachalam, S., Zeranska-Chudek, K., Zdrojek, M., Hourlier, D. (2020). Carbon-based terahertz absorbers: Materials, applications, and perspectives. *Nano Select.* 1: 471–490.

Yan, M., Zhang, D., Huizenga, J.M., Wei, J., Li, H., Li, G., Huang, X., Zhang, X., Zhao, S. (2020). Mineralogical and isotopic characterization of graphite deposits in the western part of the North Qaidam Orogen and East Kunlun Orogen, northeast Tibetan Plateau, China. *Ore Geol. Rev.* 126: 103788.

Yan, Q., Ketelboeter, T., Cai, Z. (2021). A study of the key factors on production of graphene materials from Fe-lignin nanocomposites through a molecular cracking and welding (MCW) method. *Molecules* 27: 154.

Yan, Q., Zhang, H., Ketelboeter, T., Peng, Y., Wan, C., Cai, Z. (2024). Tuning thermal and graphitization behaviors of lignin via complexation with transition metal ions for the synthesis of multilayer graphene-based materials. *RSC Adv.* 14: 7592–7600.

Yuan, Z., Hu, Z., Gao, P., Zhang, W., Tang, Y., Li, L., Shi, K., Han, S., Fan, C., Liu, J., Liu, J. (2022). Graphitic carbon nitride-derived high lithium storage capacity graphite material with regular layer structure and the structural evolution mechanism. *Electrochim. Acta.* 409: 139985.

Zhou, L., You, X., Wang, L., Qi, S., Wang, R., Uraki, Y., Zhang, H. (2023). Fabrication of graphitized carbon fibers from fusible lignin and their application in supercapacitors. *Polymers* 15: 1947.